COMPARATIVE ANALYSIS OF WATER-INDUCED RESPONSE IN 3D-PRINTED SCF/ABS COMPOSITES UNDER CONTROLLED DIFFUSION

Samiul Alam[1], Md Tareq Hassan[1], Joshua Merrell[1], Juhyeong Lee[1]
1- Utah State University
Logan, UT-84322

ABSTRACT

Additive manufacturing (AM) or 3D printing of fiber-reinforced composites (FRCs) has garnered significant interests for its versatility in creating intricate parts and rapid prototyping due to cost-effectiveness. Although short fiber-reinforced thermoplastic composites are challenging to manufacture, their mechanical properties are enhanced. However, void formation during printing is a key issue, impacting mechanical properties and facilitating water ingress, affecting long-term durability. This work studies water diffusion characteristics and the associated hydro-aging of 3D-printed short carbon fiber (SCF)/acrylonitrile butadiene styrene (ABS) composites with controlled water diffusion. Effects of material type (ABS and SCF/ABS), 3D printing path (horizontal and vertical filament orientation), and diffusion surface (uni-directional and bi-directional diffusion) on water diffusion coefficient and maximum water absorption level are characterized to ensure the long-term durability of 3D-printed ABS and SCF/ABS composites. Baseline representative volume element-based finite element (RVE-FE) diffusion models were developed based on micro-computed tomography (micro-CT) image analysis of each specimen to understand water diffusion characteristics. This work proves that the SCF/ABS composite is more resistive to hydro-aging than neat ABS due to the SCFs' hydrophobic nature. SCF/ABS composites, while providing distinct advantages over pure ABS in terms of mechanical properties, could also be more effective against moist conditions.

Keywords: 3D Printed Thermoplastic, Water Diffusion, Predictive Model
Corresponding author: Juhyeong Lee

1. INTRODUCTION

Additive Manufacturing (AM) constructs intricate geometric and material components in a layer-by-layer fashion. The precision and accuracy of this innovative manufacturing technique have made it highly sought after in the automotive, aerospace, and medical equipment industries [1]. The micro-structural characteristics of additive manufactured parts are influenced by the printing parameters and the type of AM process used [2]. AM encompasses various techniques for producing objects using polymers, such as 3D printing methods like fused deposition modeling (FDM) [3], fused filament fabrication (FFF) [4], stereolithography (SLA) [5] [6], and selective laser sintering (SLS) [7] [8].

FDM is the most common extrusion-based 3D printing method for printing both thermoplastic and thermosetting materials. FDM technology typically supports printing acrylonitrile butadiene

SAMPE Conference Proceedings. Long Beach, CA, May 20-23, 2024. Society for the Advancement of Material and Process Engineering – North America.

(DOI will be added by SAMPE)

styrene (ABS), polylactic acid (PLA), and nylon materials. FDM-printed parts are contingent upon various pivotal factors, including nozzle angles and diameters, pressure distribution, filament exit velocity [9], printing speed [10], layer height [11], and orientations [12].

Short carbon fiber reinforcements are commonly used to enhance strength, stiffness, creep resistance, thermal expansion, and toughness. However, their incorporation into FDM feedstocks introduces pores/voids in the material's microstructure, acting as stress concentration sites [13] and reducing strength. Adding short carbon fibers to PLA filaments increases voids and the risk of fiber clogging in the extruder nozzle [14]. The porosity of 3D printed carbon fiber reinforced ABS composites initially decreases with increasing carbon fiber content but eventually peaks and remains high [15]. Among 3D printed ABS, carbon nanotube (CNT)/ABS, and carbon fiber (CF)/ABS specimens with different printing directions, CF/ABS specimens have the highest porosity due to fewer bonding areas between layers and filaments [16].

The mechanical performance of carbon fiber reinforced polymer (CFRP) composites is significantly affected by hygrothermal aging. When water molecules penetrate the macro-molecular polymer networks, they disrupt the secondary bonds that hold neighboring chains together, leading to a decrease in mechanical cohesion. This results in an increase in the glass transition temperature (T_g) and leads to additive loss, material swelling/thinning, and the formation of microcracks. Water ingress has a significant impact on the adhesion of printed filaments and the interfaces between the fibers and surrounding matrix [17]. The statistical analysis reveals intricate and mutual interactions between the aging temperature and the relative humidity [18]. The rate of moisture absorption in composite is greater at an elevated temperature than a room temperature [19]. The water absorption characteristics of polymer matrix composites generally follow the principles of Fickian diffusion theory, where the flux is proportional to the diffusivity and the negative gradient of water concentration [20]. To ensure the long-term durability of 3D printed polymer matrix composites, it is necessary to apply coating systems that safeguard the surface against adverse environmental conditions. Unprotected ABS samples experience a gradual decrease in their mechanical properties (i.e., failure strain and toughness). ABS specimens coated with acrylic-styrene-acrylonitrile (ASA) effectively maintain their mechanical properties, when exposed to environmental conditions [21].

Material property degradation resulting from hydrothermal aging is influenced by various factors, including material composition, prepolymer and hardener types, reinforcements, conditioning parameters, and other material/process related parameters. Temperature and relative humidity provide additional challenges, necessitating a comprehensive approach to comprehend their impact on the integrity of materials. A mass saturation level, measured as a percentage increase in weight, quantifies the extent to which a material interacts with its surroundings. Saturation time, diffusivity, and solubility provide insights into the absorption and reaction of a material to environmental conditions. Understanding material’s inherent property changes and their contribution to long-term aging provides well-informed choices in material design and engineering.

The driving force behind our research is to understand water diffusion mechanisms of 3D-printed thermoplastic composites with and without short carbon fiber reinforcements. Previous studies have mainly addressed water and moisture absorption from all directions, however, there is a significant gap exists in understanding the diffusion characteristics in 3D printed composite

materials over controlled diffusion flow/direction (uni- or bi-direction diffusion) and the 3D printing process (vertical or horizontal printing path) for short fiber-reinforced composites. The research aimed to explore the combined effects of controlled diffusion and 3D-printing on the hydro-aging of pure ABS and SCF/ABS composites, examining water diffusion in 3D-printed specimens with horizontal and vertical orientations under uni- and bi-directional conditions. A finite element model was developed with measured diffusion parameters to gain a deeper understanding of controlled water diffusion characteristics at the microstructure scale. This study provides a comprehensive understanding of the diffusion mechanisms of 3D printed pure ABS and SCF/ABS specimens by integrating insights obtained from physical experimentation and numerical analysis.

2. EXPERIMENTATION

2.1 Specimen Preparation

ABS-M30 and ABS-CF10 (both from Stratasys) filaments were used in this study. A total of 80 cubic specimens (20 × 20 × 20) mm^3, with an equal distribution between two different printing directions: horizontal (XY) and vertical (Z), were fabricated using a Stratasys F370 printer. The nozzle moves to Z-direction after each consecutive layer printing in XY-plane (refer to Fig. 1 for coordinate system for each printing configuration). The printing was conducted at 100 % infill (solid block), with the raster angle alternating between 0° and 90° from one layer to the next. A 0.4 mm diameter printing nozzle was employed with 0.254 mm layer thickness. Figure 1 provides a visual representation of the sample geometry of ABS and SCF/ABS specimen.

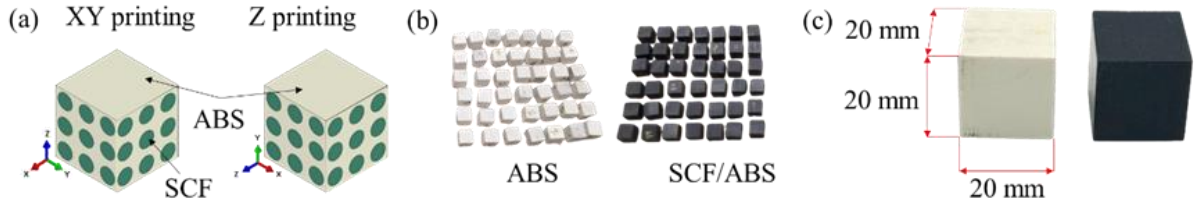

Figure 1. ABS and SCF/ABS specimens: (a) schematic of printing configuration (b) prepared specimen (c) zoomed-in view of the prepared specimen.

The water absorption properties of 3D-printed specimens are affected by both the infill percentage and the orientation of the sample during the fabrication process. Furthermore, the water diffusivity exhibits an orthotropic characteristic, specifically regarding the thickness of the layers in the printing direction. This phenomenon is attributed to the presence of interlayer porosity. To evaluate water absorption, specimens were submerged in deionized water at room temperature. For controlled water diffusion into the specimens, silicone was applied to outer surfaces of the specimens. For uni-directional (U) diffusion, five faces of both ABS and SCF/ABS specimens were coated with silicone, leaving only one face exposed to water. Similarly, for bi-directional (B) diffusion, the four faces of the specimens were coated with silicone, leaving two opposite faces exposed to water, as shown in Fig. 2. Before diffusion tests, a thorough drying process was carried out to remove any initial moisture present in the samples. Following a 24-hour curing period, the specimens covered with silicone were subjected to a 48-hour drying process in an oven set at 70°C. Afterwards, all specimens were weighed, and the measurements were recorded. Table 1 includes a total number of specimens prepared for each test configuration.

(a) Uni-directional Diffusion (b) Bi-directional Diffusion

Figure 2. Silicon coated ABS (white) and SCF/ABS (black) specimens for: (a) uni-directional and (b) bi-directional water diffusion tests.

Table 1. Number of specimens for ABS and SCF/ABS specimen for each testing configuration

Material	**ABS**					**SCF/ABS**				
Configuration	SBXY	SBZ	SUXY	SUZ	Total	SBXY	SBZ	SUXY	SUZ	Total
Specimens	10	10	10	10	40	10	10	10	10	40

Note: SBXY = Horizontally printed (XY) specimen under bi-directional (B) diffusion, SUXY = Horizontally printed (XY) specimen under uni-directional (U) diffusion, SBZ = Vertically printed (Z) specimen under bi-directional (B) diffusion, SUZ = Vertically printed (Z) specimen under uni-directional (U) diffusion.

2.2 Water Diffusion Experiment

Water diffusion tests continued until three consecutive weight measurements recorded an average water gain in mass of no more than 1 % or 5 mg, whichever value was greater, in accordance with ASTM D570 [22]. During the tests, the specimens were regularly extracted, and cleaned with dry paper towels, and their weights were measured. The change in weight (M_t) of a specimen due to water diffusion can be determined using Eqn. 1.

$$M_t(t) = \frac{W_t - W_0}{W_0} \times 100\ \% \qquad [1]$$

where W_t is the wet weight at time t, and W_0 is the dry weight.

2.3 Microstructural Observation

A micro-computed tomography (micro-CT) examination was performed on both types of specimens utilizing the Nikon XT H 225 ST MRA Dual Target scanner. In essence, micro-CT image analysis provides useful information, such the geometry and dimensions for representative volume element (RVE) based finite element models, as well as microstructure changes of specimens after being exposed to water. The micro-CT images were obtained with the following parameters: an X-ray tube voltage of 85 kV, a current of 153 μA, a resolution set at 13.77 μm for the voxel edge size, 7000 projections, and a complete 360º imaging rotation lasting 4 hours. The extensive dataset consisting of 7000 projections and a complete 360º rotation offers a three-dimensional (3D) perspective of the microstructural characteristics of the specimen.

2.4 Experimental Results

2.4.1 Absorption Properties

Figure 3 shows the evolution of water absorption, measured by a weight increase, of neat ABS specimens under both uni- and bi-directional water diffusion. At an early stage of water diffusion, SBZ and SUZ specimens exhibited similar water absorption trends. Over time, SBZ specimens showed a rapid increase in water absorption and stabilized to 8.50% after ~170 hours. It is important to note that water absorption in Fig. 3 is plotted with respect to the square root of time, thus ~13hr in the x-axis of the figure corresponds to the square root of ~170 hours. SUZ specimens reached their highest level of water absorption relatively earlier at approximately 90 hours and then showed a steady increase in water absorption, reaching the maximum saturation levels (9.54%) similar to those observed in SBZ specimens. SBXY specimens demonstrated a weight increase of up to approximately 6%, whereas SBZ specimens showed a higher maximum water saturation around 10%. The water absorption for SUZ specimens exhibited a higher standard deviation compared to SBZ specimens. This can be attributed to the presence of random and extensive void distributions within the specimens, which introduce variability in their water absorption behavior. As the diffusion occurs from one face in SUZ, this randomness has a higher impact on creating variability than the SBZ specimen where the diffusion occurs from both faces, providing a more uniform diffusion. In addition, horizontally printed specimens that have uni-directional (SUXY) and bi-directional (SBXY) water diffusion consistently showed that SUXY specimens absorbed a slightly greater amount of water than SBXY. These different water absorption characteristics became increasingly evident after approximately 455 hours. Note that note that the scale of the x-axis is given in the square root of time, thus 455 hours correspond to ~21 hours in Fig. 3a.

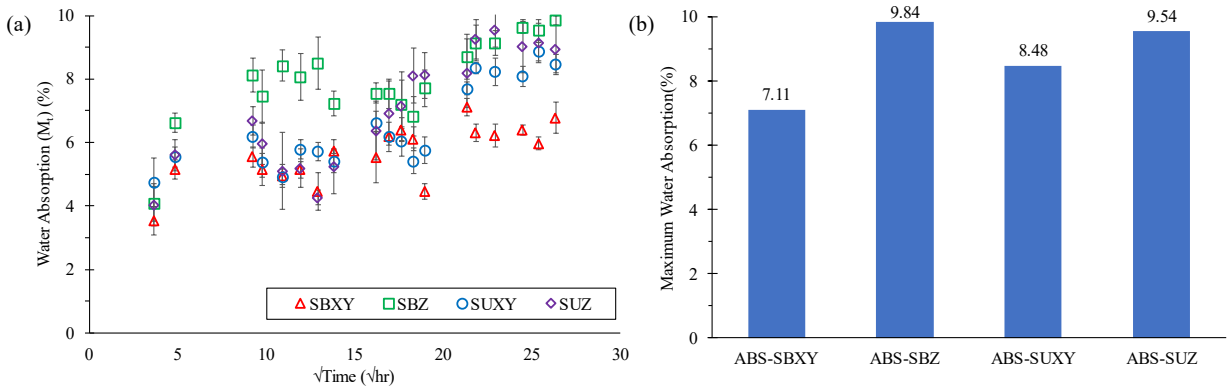

Figure 3. Water diffusion test results: (a) water absorption (%) and (b) maximum water absorption level (%) of 3D-printed ABS specimens.

The SCF/ABS specimens demonstrated slightly reduced water absorption levels, underscoring the impeding influence of SCFs on water diffusion (Fig. 4). Carbon fibers are hydrophobic in nature, thus the presence of SCF into ABS matrix plays a pivotal role to resist the water diffusion into the SCF/ABS specimen. This resistance to water diffusion is greater in the transverse direction to the fiber than along the fiber direction, as there is a more organized pathway for the water to diffuse in the fiber direction. SUZ specimens absorbed a greater amount of water than SBZ specimens. This observation underscores the significance of unidirectional flow in augmenting water uptake.

The vertical printing configurations (SUZ and SBZ) consistently exhibit greater water absorption compared to their horizontally printed counterparts (SUXY and SBXY). This implies that printing path has substantial influence on water diffusion characteristics, whereby unidirectional flow specifically enhances water absorption. Comparing the horizontal and vertical printing orientations in SCF/ABS composites, both SUZ and SBZ specimens exhibited lower water absorption compared to SUXY and SBXY specimens. This trend highlights the significance of the influence of 3D printing on water absorption characteristics, which is determined by the path followed during the printing process. The weight gain percentages provide additional clarity to these observations, with SBXY showing a 6% increase, SUZ exhibiting an 8% increase, and both values indicating lower overall water absorption, compared to pure ABS specimens. The decrease in overall water absorption can be ascribed to the impediment caused by carbon fibers on the diffusion of water in SCF/ABS. Furthermore, the SCF/ABS specimens showed smaller variations in each measurement, indicating more consistent water diffusion responses than pure ABS specimens over time.

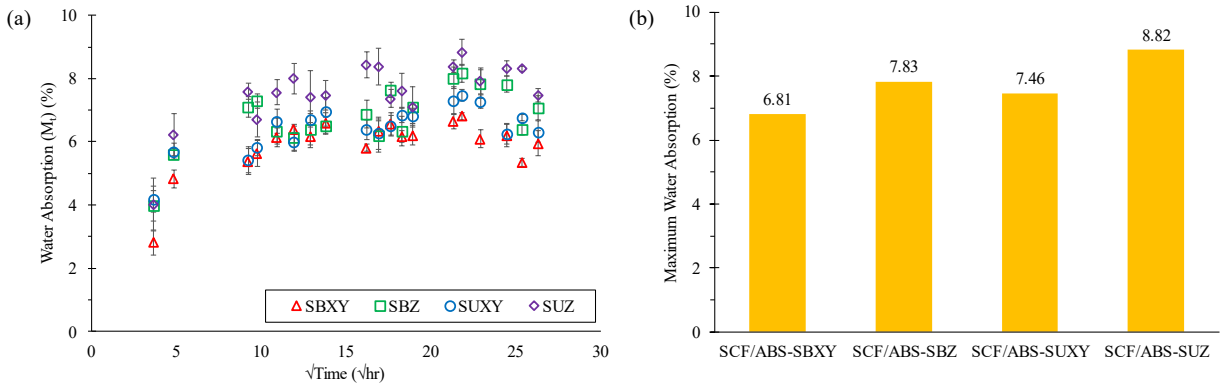

Figure 4. Water diffusion test results: (a) water absorption (%) and (b) maximum water absorption level (%) of 3D-printed SCF/ABS specimens.

The diffusivity is contingent upon the diffusion length/distance. In all circumstances, whether it is uni- or bi-directional diffusion, the diffusion length is equal to the entire width of the specimen. The increased water absorption of the SUXY and SUZ specimens can be attributed to the fact that the coated faces opposite to the diffusion face function as a chamber to store more water within the specimen via unidirectional diffusion. In bi-directional diffusion, the presence of two opposed open faces initially results in a higher absorption rate. However, it also permits some water to diffuse through the other face, across the entire width. Consequently, the overall water absorption is reduced.

The maximum absorption difference of 0.7% between pure ABS and SCF/ABS specimens in SBXY indicates that SCF reinforcement has a relatively minor effect on water uptake in the horizontal printing configuration. In contrast, SBZ configuration demonstrates a more noticeable disparity, reaching 1.7%, highlighting a significant impact of carbon fibers in the vertical printing orientation. SUXY exhibits a 1.0% disparity in the horizontal plane, whereas SUZ displays a 1.4% fluctuation in the vertical configuration.

2.4.2 Microstructural Observations

Utilizing the projections obtained from the micro-CT scanner, comprehensive 3D image analysis of representative microstructures of ABS and SCF/ABS specimens was generated through VGStudio Max 3.5. Notably, distinct transformation in filament shape was observed, shifting from circular to elliptical cross-sections after deposition on the printing bed. This alteration was consistent for both ABS and SCF/ABS specimens, where subsequent expansion occurred. It is crucial to highlight that irregularly shaped voids are inherent within micro-structures due to temperature and pressure gradients between each deposited layer of both specimens. These voids serve as primary reservoirs for storing water within the specimens, consequently contributing to an increase in water diffusion.

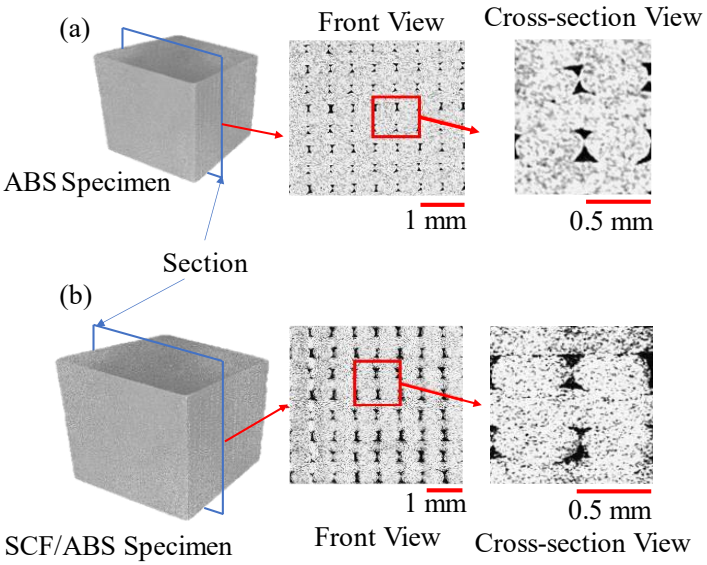

Figure 5. Micro-CT images of (a) ABS and (b) SCF/ABS specimens after water diffusion.

Figure 5 shows representative micro-CT images obtained from the ABS and SCF/ABS specimen showing key microstructural features. In the figure, ABS (matrix) is shown in white, voids are in black. Differentiating the SCFs from the ABS matrix is difficult due to the comparable density of the two materials, however, it is safe to assume that the SCF's retains their same shape and size in the ABS specimen, and they are oriented in the printing direction. The micro-CT image analyses highlight significant differences in the geometric characteristics of the neat ABS and SCF/ABS specimens. While the overall shapes of cross section of the deposited filament are comparable, there are slight variations in the dimensions of the filaments. More precisely, the ABS specimen (Fig. 5a) contains filaments with smaller elliptical cross-sections, compared to the SCF/ABS specimen (Fig. 5b). As the pure ABS has a fairly homogeneous matrix, the consolidation and solidification are more uniform than the SCF/ABS matrix which aids the smaller cross-sectional area of the filament. In addition, the ABS specimen exhibits relatively large triangular-shaped voids that are similarly aligned, primarily occurring between the beads deposited during the printing process. The circular nozzle applies pressure to the molten material, and as the top part cools, it forms rounded edges before another layer is added on top. This causes any gaps to be directed downwards, resulting in inter-bead pores. However, for the SCF/ABS specimen, the voids within the filament begin to form due to the stress concentration at the tip of the short carbon fibers.

But the higher thermal conductivity of the carbon fiber enables a more even dispersion of heat that is released as the specimen cools down after filament deposition on the printing bed. SCFs cause a decrease in the average size of triangular channels by reducing die-swell and increasing thermal conductivity. In addition, their higher thermal conductivity facilitates the softening of bottom beads that have already cooled when they encounter a hot bead being deposited on top. This results in more compaction and smaller overall voids in the SCF/ABS specimen. This phenomenon substantiates the noted disparities in filament dimensions and void sizes between pure ABS and SCF/ABS specimens.

3. NUMERICAL STUDY

3.1 Fickian Diffusion

The Fickian diffusion model [23] is a mathematical framework that explains the mechanism of mass transport, where the movement of a substance through a medium is driven by the concentration gradient. This model is particularly useful for understanding the movement of water molecules within materials over time. The proposition asserts that the rate of water diffusion (flux) is intrinsically connected to the concentration gradient, which represents the process by which substances migrate from areas of greater concentration to those of lesser concentration. The Fickian diffusion model is based on the idea that particles experience random thermal motion and move from regions of higher concentration to regions of lower concentration to equalize the concentrations. This model functions as a valuable instrument for predicting water diffusion patterns in various materials as well as improving the development of composite materials. The Fickian model typically exhibits a linear slope (representing diffusivity) followed by saturation.

The solution of a 1D Fick's diffusion model [23] is given as:

$$C_t = \frac{M_t}{M_\infty} = 1 - \frac{8}{\pi^2}\sum_{i=0}^{\infty}\frac{1}{(2i+1)^2}exp^{\left(\frac{-(2i+1)^2\pi^2 D_n t}{{h_n}^2}\right)} \quad [2]$$

Where C_t is the concentration, M_t is the water absorption at time t, M_∞ is the maximum water uptake, D_n is the water diffusion coefficient, and h_n is the thickness of specimen.

The water diffusion coefficient (D_n) of each specimen was determined by fitting the analytical model (Eqn. 6) to the experiment data. An in-house MATALB code was developed to calculate water diffusion coefficients that provides a detailed characterization and understanding of the intricate dynamics of water diffusion within the material.

The diffusion parameters acquired from experiments are provided in Table 2. The M_{inf} is the maximum water absorption and D is calculated using the 1D Fickian diffusion coefficient equation (Equation 6.) applying MATLAB model.

Table 2. Diffusion parameters for numerical analysis of pure ABS and SCF/ABS specimen

Sample	Pure ABS	SCF/ABS

Path		SBXY	SBZ	SUXY	SUZ	SBXY	SBZ	SUXY	SUZ
1D Fick Model	D (mm^2/hr)	0.0013	0.0004	0.0045	0.0006	0.0009	0.0005	0.0037	0.0012
	M_{inf} (%)	7.16	9.81	8.52	9.55	6.82	7.86	7.48	8.85
Experiment	M_{inf} (%)	7.11	9.84	8.48	9.54	6.81	7.83	7.46	8.82

3.2 RVE Modeling

Figure 6 displays the finite element (FE) mesh of water diffusion analyses developed for ABS and SCF/ABS specimens developed using Abaqus 2022 [24]. RVE model dimensions determined from micro-CT images are included in Table 3. The SCF/ABS RVE model (Fig. 6b) has SCF volume fraction V_f =6 %. The SCF has a 7.5 µm diameter and a length of 100 µm oriented in the printing direction. The measurements for ABS and SCF/ABS can be found in Table 3. W represents the alignment of SCF reinforcements in the printing direction, with a length that is twice the normal length of SCF to accommodate two full reinforcements. In this work, several assumptions were made for geometric simplicity, including (1) a perfect bonding between SCFs and ABS and (2) SCFs with random orientation within the filament along the printing direction, and (3) no voids within filaments.

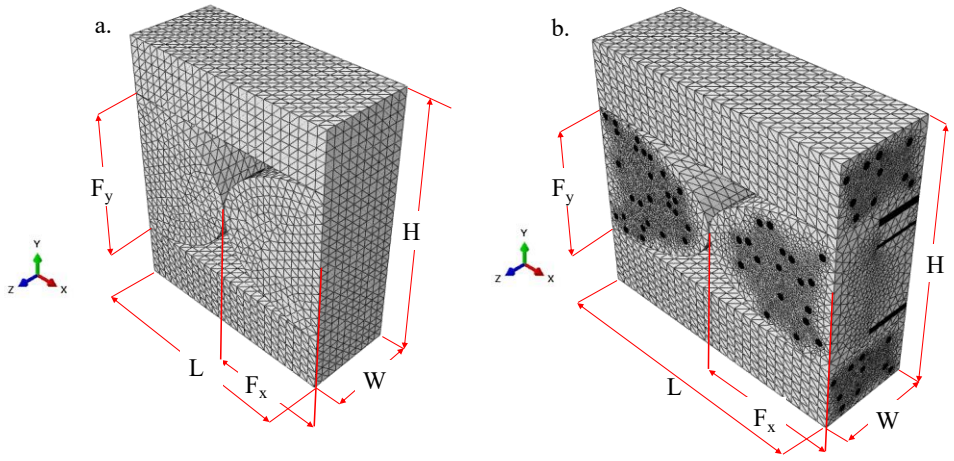

Figure 6. Representative Volume Element (RVE) for a. pure ABS b. SCF/ABS specimen.

Table 3. The dimensions of RVE model acquired from micro-CT observation.

Specimen	**L (mm)**	**H (mm)**	**W (mm)**	**F_x (mm)**	**F_y (mm)**
Pure ABS	0.49	0.575	0.2	0.245	0.33
SCF/ABS	0.57	0.53	0.2	0.285	0.27

3.3 Finite Element (FE) Model development

Following a mesh sensitivity study, a global element size of 10 µm was determined for pure ABS, and DC3D4 (tetrahedral) elements were employed. The total number of elements utilized was 297,961 for ABS specimen. For SCF/ABS, the global element size was 40 µm, however, smaller element size was taken near the SCF region to increase the accuracy of the analysis, a total of 877,646 elements were generated. A total diffusion period of 15 hours was simulated, given the small size of the RVE model. A maximum allowable normalized concentration changes of 1% was set, ensuring the accuracy of the computational results. Boundary conditions were as follows: no flux boundary condition ($J = 0$), normalized concentration boundary condition ($\varphi = 1$). The diffusion process occurred from $\varphi = 1$ towards lower concentrations ($\varphi = 0$), creating a realistic and controlled computational environment for the diffusion analyses.

3.4 Model Prediction

Figures 7 and 8 demonstrate the normalized nodal concentration of water after 1, 5, and 15 hours of water diffusion for unidirectional and bi-directional water diffusion of ABS and SCF/ABS specimen, respectively. For vertically printed ABS specimen (SBZ and SUZ), the water concentration is higher than horizontally printed specimen (SBXY and SUXY), however, the diffusion rate is comparatively slower in both uni-directional (SUXY and SUZ) and bi-directional (SBXY and SBZ) diffusion. This trend is applicable for the SCF/ABS specimen too. The larger diffusion surface in horizontally printed specimen is the reason behind this trend. Furthermore, the incorporation of SCFs in the SCF/ABS specimens hinders the movement of water diffusion, especially when the fibers are oriented perpendicular to the direction of diffusion. The presence of vertically oriented fibers in the ABS matrix (SBZ and SUZ) significantly increases the resistance to water flow in a direction perpendicular to the fibers, thereby acting as effective barriers to diffusion.

The variation in diffusion characteristics between ABS and SCF/ABS specimens becomes more prominent as the time passes. Initially, the NNC contours between ABS and SCF/ABS specimen are comparable at 1 hour. The SUXY and SBXY specimen has a very little difference in concentration while SBZ and SUZ specimen show similar concentration in ABS and SCF/ABS specimen. The presence of carbon fibers or the variation of printing configurations starts to play their role as the diffusion time increases. At 5 hours of diffusion time, it can be seen that the diffusion rate is comparatively higher in the SCF/ABS than ABS specimen in all configurations. The water travelled at a larger distance in SCF/ABS specimen than it did in ABS specimen. This is due to a more uniform pathway for the water to diffuse in the SCF/ABS specimen in the presence of short carbon fibers. However, as the triangular voids are smaller in the SCF/ABS specimen than the ABS, the concentration is still smaller in the SCF/ABS specimen. After 15 hours of diffusion, the difference in absorption contour between SCF/ABS and ABS is very significant. The SCF/ABS-SBXY specimen is fully saturated with the maximum water concentration while the ABS-SBXY specimen has similar contour as it was after 5 hours. Although the concentration level for the ABS-SBXY is smaller than the SCF/ABS-SBXY specimen, this suggests that SCF/ABS specimen (SBXY) will reach its saturation point much faster than the ABS one. This trend is applicable to the specimens in other configurations too. In the case of SBZ, SUXY, and SUZ specimens, the concentration level is lower in the SCF/ABS specimens, but the diffusion rate is higher. So, it can be deducted that while the presence of SCF helps to resist the water diffusion,

the time required to reach the saturation level for SCF/ABS specimen is much lower than the ABS specimen.

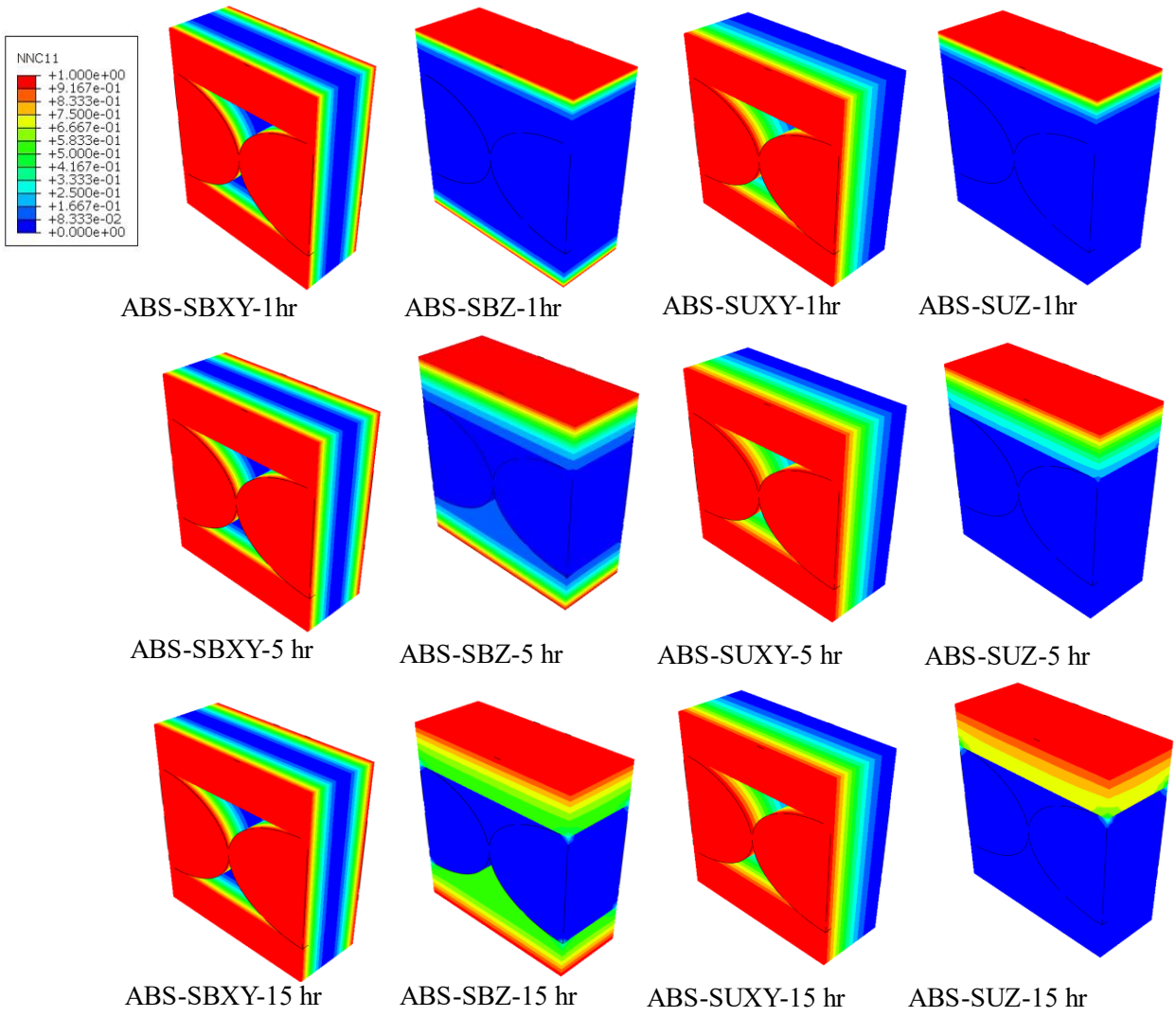

Figure 7. Predicted Normalized Nodal Concentration (NNC) contours after 1, 5 and 15 hours for ABS specimen subjected to controlled water diffusion.

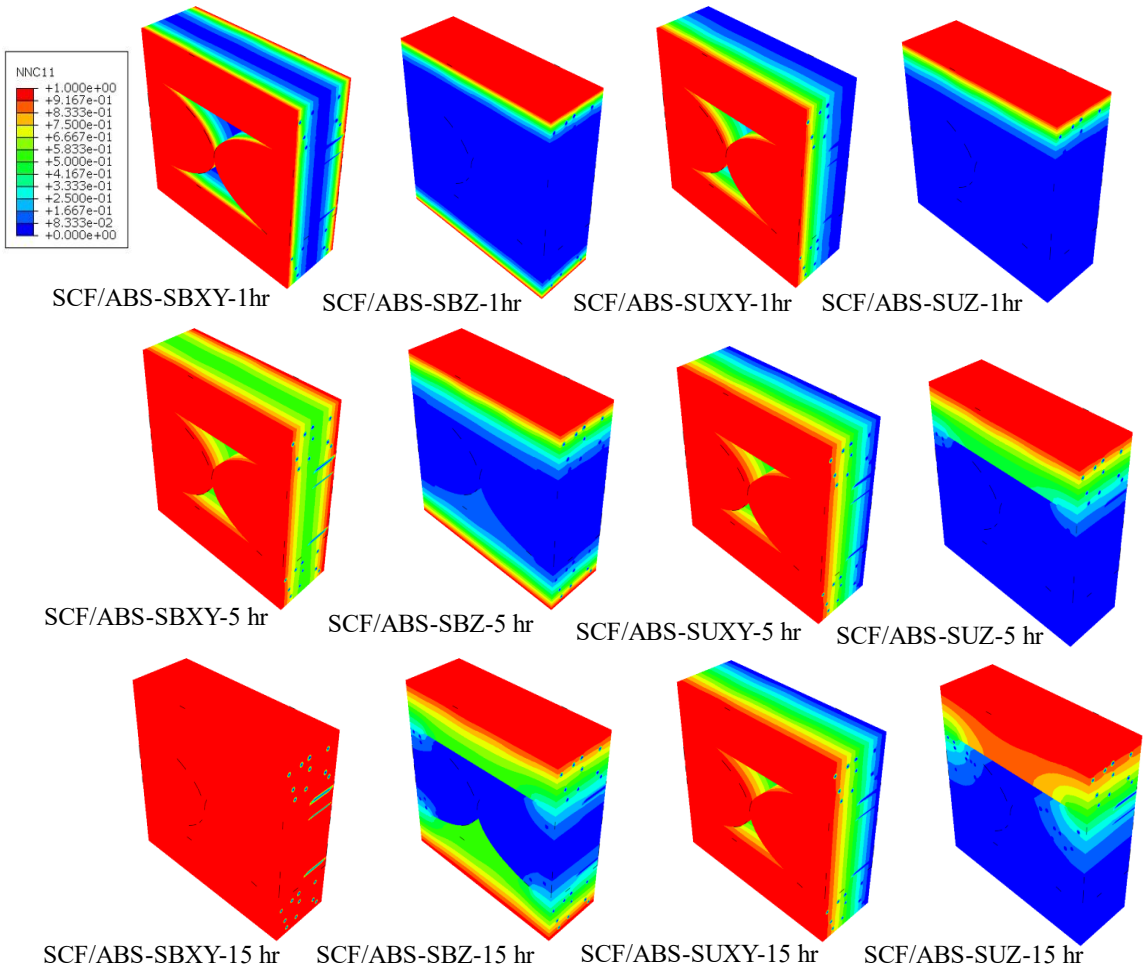

Figure 8. Predicted Normalized Nodal Concentration (NNC) contours after 1, 5 and 15 hours for SCF/ABS specimen subjected to controlled water diffusion.

4. CONCLUSIONS

This study highlights the effects of several material and process parameters on hydro-aging characteristics of 3D-printed ABS and SCF/ABS composites. The water absorption rate is found to be influenced significantly by two key parameters: the 3D printing path, specifically the orientation (vertical versus horizontal), and the direction of diffusion (uni- versus bi-directional diffusion). Coating the specimen with silicon on all faces except the desired diffusion face. Findings show that SCF/ABS specimen printed in horizontal direction retains the lowest water content (6.8 %) while the neat ABS printed in vertical fashion displays the highest water absorption (9.84 %) under bi-directional diffusion. SCF/ABS specimen always shows a better resistance to water absorption in all printing orientation and diffusion direction. This initial exploration demonstrates the potential for controlled hydro-aging of 3D-printed composites, with short carbon fibers (SCFs) emerging as effective resistors against water diffusion and absorption within the material. Ongoing investigations in our laboratory aim to delve deeper into various aspects, including the influence of diffusion temperature, environmental conditions (pH), and other external factors as the effects of specimen size and shape.

5. ACKNOWLEDGEMENT

This work was supported in part by the National Science Foundation (NSF) Advancing Sustainability Through Powered Infrastructure for Roadway Electrification (ASPIRE) Engineering Research Center under Grant EEC-1941524.

6. REFERENCES

[1] A. Gupta, S. Hasanov, and I. Fidan, "Processing and Characterization of 3d-Printed Polymer Matrix Composites Reinforced with Discontinuous Fibers." *International Solid Freeform Fabrication Symposium*, 2019, University of Texas at Austin.

[2] H. Ramezani Dana, F. Barbe, L. Delbreilh, M. Ben Azzouna, A. Guillet, and T. Breteau, "Polymer additive manufacturing of ABS structure: Influence of printing direction on mechanical properties," *J Manuf Process*, vol. 44, pp. 288–298, Aug. 2019, doi: 10.1016/J.JMAPRO.2019.06.015.

[3] R. Singh and H. K. Garg, "Fused Deposition Modeling – A State of Art Review and Future Applications," *Encyclopedia of Smart Materials*, pp. 270–288, Jan. 2016, doi: 10.1016/B978-0-12-803581-8.04037-6.

[4] J. Nomani, D. Wilson, M. Paulino, and M. I. Mohammed, "Effect of layer thickness and cross-section geometry on the tensile and compression properties of 3D printed ABS," *Mater Today* Commun, vol. 22, p. 100626, Mar. 2020, doi: 10.1016/J.MTCOMM. 2019.100626.

[5] F. P. W. Melchels, J. Feijen, and D. W. Grijpma, "A review on stereolithography and its applications in biomedical engineering," *Biomaterials*, vol. 31, no. 24, pp. 6121–6130, Aug. 2010, doi: 10.1016/J.BIOMATERIALS.2010.04.050.

[6] K. Salonitis, "Stereolithography," *Comprehensive Materials Processing*, vol. 10, pp. 19–67, Jan. 2014, doi: 10.1016/B978-0-08-096532-1.01001-3.

[7] J. Bai, B. Zhang, J. Song, G. Bi, P. Wang, and J. Wei, "The effect of processing conditions on the mechanical properties of polyethylene produced by selective laser sintering," *Polym Test*, vol. 52, pp. 89–93, Jul. 2016, doi: 10.1016/J.POLYMERTESTING .2016.04.004.

[8] P. Peyre, Y. Rouchausse, D. Defauchy, and G. Régnier, "Experimental and numerical analysis of the selective laser sintering (SLS) of PA12 and PEKK semi-crystalline polymers," *J Mater Process Technol*, vol. 225, pp. 326–336, Nov. 2015, doi: 10.1016/J.JMATPROTEC.2015.04.030.

[9] M. S. M. N. Khan, S. Alam, and M. A. Al Bari, "Numerical Analysis of Thermal Behavior of 3D Printing Nozzle Arrangement," *International Conference on Mechanical Engineering and Applied Sciences*, Dec 2022, Military Institute of Science and Technology.

[10] P. Rezaeian, M. R. Ayatollahi, A. Nabavi-Kivi, and N. Razavi, "Effect of printing speed on tensile and fracture behavior of ABS specimens produced by fused deposition modeling," *Eng Fract Mech*, vol. 266, p. 108393, May 2022, doi: 10.1016/J. ENGFRACMECH.2022.108393.

[11] S. W. Ahmed et al., "On the effects of process parameters and optimization of interlaminate bond strength in 3D printed ABS/CF-PLA composite," *Polymers*, vol. 12, no. 9, Sep. 2020, doi: 10.3390/POLYM12092155.

[12] N. Markiz, E. Horváth, and P. Ficzere, “Influence of printing direction on 3D printed ABS specimens,” *Production Engineering Archives*, vol. 26, no. 3, pp. 127–130, Sep. 2020, doi: 10.30657/pea.2020.26.24.

[13] H. L. Tekinalp, V. Kunc, G. M. V. Garcia, C. E. Duty, L. J. Love, A. K. Naskar, C. A. Blue, S. Ozcan, “Highly oriented carbon fiber–polymer composites via additive manufacturing,” *Compos Sci Technol*, vol. 105, pp. 144–150, Dec. 2014, doi: 10.1016/J.COMPSCITECH.2014.10.009.

[14] M. Ivey, G. W. Melenka, J. P. Carey, and C. Ayranci, “Characterizing short-fiber-reinforced composites produced using additive manufacturing,” *Advanced Manufacturing: Polymer and Composites Science*, vol. 3, no. 3, pp. 81–91, Jul. 2017, doi: 10.1080/20550340.2017.1341125.

[15] F. Ning, W. Cong, J. Qiu, J. Wei, and S. Wang, “Additive manufacturing of carbon fiber reinforced thermoplastic composites using fused deposition modeling,” *Compos B Eng*, vol. 80, pp. 369–378, Oct. 2015, doi: 10.1016/J.COMPOSITESB.2015.06.013.

[16] W. Zhang et al., “Interfacial bonding strength of short carbon fiber/acrylonitrile-butadiene-styrene composites fabricated by fused deposition modeling,” *Compos B Eng*, vol. 137, pp. 51–59, Mar. 2018, doi: 10.1016/J.COMPOSITESB.2017.11.018.

[17] B. C. Kikuchi, F. L. de S. Bussamra, M. V. Donadon, R. T. L. Ferreira, and R. de C. M. Sales, “Moisture effect on the mechanical properties of additively manufactured continuous carbon fiber-reinforced Nylon-based thermoplastic,” *Polym Compos*, vol. 41, no. 12, pp. 5227–5245, Dec. 2020, doi: 10.1002/pc.25789.

[18] M. Haghighi-Yazdi, J. K. Y. Tang, and P. Lee-Sullivan, “Moisture uptake of a polycarbonate blend exposed to hygrothermal aging,” *Polym Degrad Stab*, vol. 96, no. 10, pp. 1858–1865, Oct. 2011, doi: 10.1016/j.polymdegradstab.2011.07.007.

[19] A. D. Banjo, V. Agrawal, M. L. Auad, and A. D. N. Celestine, “Moisture-induced changes in the mechanical behavior of 3D printed polymers,” *Composites Part C: Open Access*, vol. 7, p. 100243, Mar. 2022, doi: 10.1016/J.JCOMC.2022.100243.

[20] E. Kim, Y. J. Shin, and S. H. Ahn, “The effects of moisture and temperature on the mechanical properties of additive manufacturing components: Fused deposition modeling,” *Rapid Prototyp J*, vol. 22, no. 6, pp. 887–894, 2016, doi: 10.1108/RPJ-08-2015-0095.

[21] A. Afshar and R. Wood, “Development of weather-resistant 3d printed structures by multi-material additive manufacturing,” *Journal of Composites Science*, vol. 4, no. 3, 2020, doi: 10.3390/jcs4030094.

[22] ASTM D570-98, Standard Test Method for Water Absorption of Plastics, *ASTM International*, West Conshohocken, PA, 1998.

[23] Crank, John, “The Mathematics of Diffusion”, *Oxford University Press*, 1975.

[24] Abaqus Inc. “Abaqus user’s manual”. *ABAQUS Inc., Dassault Systemes*, Rhode Island, USA.